J Nanopart Res (2016) 18:239
DOI 10.1007/s11051-016-3548-1

RESEARCH PAPER

Influence of the synthesis conditions of gold nanoparticles on the structure and architectonics of dipeptide composites

Alexander I. Loskutov · Olga A. Guskova · Sergey N. Grigoriev · Vadim B. Oshurko · Aleksei V. Tarasiuk · Olga Ya. Uryupina

Received: 5 May 2016 / Accepted: 1 August 2016 / Published online: 12 August 2016

Abstract A wide variety of peptides and their natural ability to self-assemble makes them very promising candidates for the fabrication of solid-state devices based on nano- and mesocrystals. In this work, we demonstrate an approach to form peptide composite layers with gold nanoparticles through in situ reduction of chloroauric acid trihydrate by dipeptide and/or dipeptide/formaldehyde mixture in the presence of potassium carbonate at different ratios of components. Appropriate composition of components for the synthesis of highly stable gold colloidal dispersion with particle size of 34–36 nm in dipeptide/formaldehyde solution is formulated. Infrared spectroscopy results indicate that dipeptide participates in the reduction process, conjugation with gold nanoparticles and the self-assembly in 2D, which accompanied by changing peptide chain conformations. The structure and morphology of the peptide composite solid layers with gold nanoparticles on gold, mica and silica surfaces are characterized by atomic force microscopy. In these experiments, the flat particles, dendrites, chains, mesocrystals and Janus particles are observed depending on the solution composition and the substrate/interface used. The latter aspect is studied on the molecular level using computer simulations of individual peptide chains on gold, mica and silica surfaces.

Keywords Gold nanoparticles · Peptide · Morphology · Nanocomposite · Synthesis · Nanoscale architechture

A. I. Loskutov (✉) · S. N. Grigoriev · V. B. Oshurko
Moscow State Technological University STANKIN, Vadkovskii per. 1, Moscow, Russia 127994
e-mail: ailoskutov@yandex.ru

O. A. Guskova
Leibniz Institute of Polymer Research Dresden, Hohe Str. 6, 01069 Dresden, Germany

O. A. Guskova
Dresden Center for Computational Materials Science (DCMS), Technische Universität Dresden, 01062 Dresden, Germany

A. V. Tarasiuk
FSBI "Zakusov Institute of Pharmacology", Russian Academy of Medical Sciences, Baltiyskaya str. 8, Moscow, Russia 125315

O. Ya. Uryupina
Frumkin Institute of Physical Chemistry and Electrochemistry, Russian Academy of Sciences, Leninskii pr. 31, Moscow, Russia 119991

Introduction

Recent advances in nanoscience and nanotechnology, particularly the development of new nanocomposite materials and coatings have increased concerns regarding the risks they may have on human health or the environment. Current methods for the synthesis of inorganic nanostructures have serious drawbacks, involving hazardous and toxic reactants, synthesis

under extreme conditions of temperature, pressure, pH or salinity. By contrast, biological systems allow for synthesis of nanostructures in an environmental benign way using eco-compatible reagents according to one of the concepts of Green Chemistry by Marteel-Parrish and Abraham (2013). The use of biomimetic components such as amino acids (Lerner 2004; Dahl et al. 2007) or synthetic peptides (PTs) (Brorsson et al. 2010) provides an additional possibility to control the synthesis and self-assembly of functional nanocomposite structures.

The size of nanoparticles (NPs) makes them ideal candidates for the fabrication of new "smart" materials. On the other hand, their biocompatibility can be tuned using polypeptides. The latter possess various chemical structures, are chemically and thermally stable, and pH-sensitive. Besides, PTs exhibit a high binding affinity to inorganic surfaces including metals, and therefore can be successfully used for the synthesis of various hybrid nanostructures and coatings. It was recently demonstrated that PT solid-state coatings possess enhanced adhesion strength, anti-friction properties and hardness, which depend on the conformation of the polypeptide chains in adsorption layers (Prokopovich and Starov 2011). For instance, the hardness of some self-assembled PT fibrils is characterized by extremely high values up to 20 GPa (Knowles and Buehler 2011).

Much research on PTs has been carried out to maintain their structure and biological function in a liquid phase which is in focus of medicine and molecular biology. In contrast, for the formulation of functional biomimetic nanomaterials, PTs usually are considered as active thin films on a solid support, for example for biosensors or electronic applications. Despite the fact that these organic/inorganic interfaces determine the device properties, both the PT binding to the substrates and the formation of coatings are still poorly understood, in particular with regard to the structural and electronic properties of such interfaces. The interactions at the interfaces depend on several important factors: the surface chemistry, its nanotopography and the strength of intermolecular interactions. For the practical applications of PT-based composite materials, such aspects as how to control the degradation or to maintain the stability also play a very important role (Loskutov et al. 2013a).

For instance, assemblies consisting of amyloid-type PTs (Loskutov et al. 2013b; Loskutov et al. 2015) can be used as a promising component of new solid-state bio-inspired functional materials, as well as anti-friction coatings for MEMS/NEMS devices. Our previous studies have shown that PT composite materials and coatings with silver and gold NPs exhibit structural, electro-physical and tribological properties that make them promising for large-scale practical applications (Loskutov et al. 2013b, 2015). In these studies, we used a new dipeptide (DPT) which belongs to a class of short neuroprotection PTs (Seredenin and Gudasheva 2011). We suppose it could be used not only for medical applications, but also as a perspective functional material for organic electronics. On the other hand, the combination of DPT with gold NPs might reveal previously unknown pharmacological properties of composite materials.

In the development of advanced smart materials, the control of morphology plays a major role because the latter determines the functional properties of the materials. To understand the structure–property interrelation, a high level of understanding of the underlying processes and mechanisms is required which in turn depend on the conditions of materials synthesis.

The simultaneous formation of the NPs and their self-assembly with PTs on surfaces into ordered ensembles is considered one of the most important questions in formulation of bio-inspired nanoarchitectonics for a variety of reasons. First of all, the driving forces behind these processes are caused by a gentle interplay between different intermolecular non-covalent bonds, including organic/inorganic, organic/organic and adsorbent/substrate interactions (Grzybowski 2014). Secondly, the self-organization occurs on different time and length scales. Here, particularly difficult case is to drive the assembly of primary NPs into different 3D mesocrystals of micron size (Bahrig et al. 2014; Polte 2015). We have recently demonstrated exemplary mesostructured growth of solid-state PT composite layers with silver NPs (Loskutov et al. 2013b), where regular-shaped isolated tetrahedrons with sides up to 30 μm in length and more than 5 μm in height were observed. This process was substantially dependent on the chemical nature and geometry of the substrate, as well as on the NPs used.

The next aspect of supramolecular nanoarchitectonics is rational design of intrinsic structure of the molecular building blocks. However, the properties of materials are finally defined at the macroscopic level, and the relationship between chemical composition

and macroscopic action of matter remains a hot topic of modern nanoscience (Ariga et al. 2016). Although recent studies have uncovered a morphological diversity of PT solid layers and related effects, e.g. polymorphism (Conejero-Muriel et al. 2015; Bedford et al. 2016; Karki et al. 2015), there are still many unknowns yet to be resolved. Further progress on the characterisation of the PT composite layers and its incorporation into the computer simulation framework is expected to shed additional light on the role of interfacial interactions and the structure–property relationships.

The main goal of this work is to link the molecular structure of the DPT chains during the synthesis of gold NPs composites and the morphology of the resulting solid-state nanocomposite layers. In order to achieve our goal, we have established the following specific objectives: (i) to develop a one-step synthesis of gold NPs in the DPT environment, prepare monodisperse and stable Au-NPs, (ii) to study the PT self-assemblies on different substrates and (iii) to investigate the influence of different factors such as ratio of components, pH, the nature of the substrate and deposition method used on the processes of crystallization and growth of large mesocrystals. We believe that our results will be particularly useful for gaining a deeper understanding of the systems under study and would allow for further development of various PT/NPs nanocomposites with prescribed properties.

The remainder of this paper is organized as follows: "Experimental section" describes the experimental methods for the synthesis of NPs and preparation of solid films, the morphological characterisation and computer simulation of interfacial interactions. Results are presented in "Results" section, which is followed in "Conclusions" section by final conclusions and directions for future work.

Experimental section

Dipeptide bis-(N-monosuccinyl-L-glutamyl-L-lysine) hexamethylenediamide, $\{HOOC–(CH_2)_2–CO–Glu–Lys–NH–(CH_2)_3–\}_2$, $M_w = 830{,}9$ Da, pH = 4.2 (0.1 %wt aqueous solution) were synthesized at the FSBI "Zakusov Institute of Pharmacology" (Russia), (Fig. 1) (Seredenin and Gudasheva 2011; Povarnina et al. 2013).

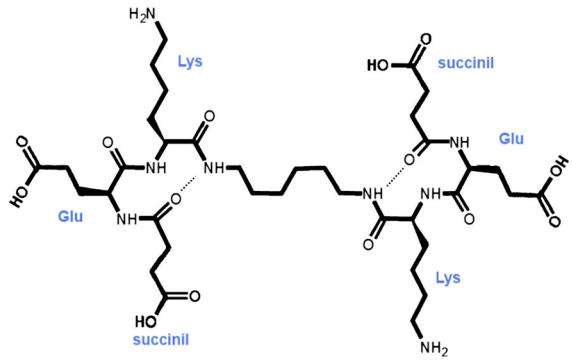

Fig. 1 Structure of dipeptide molecule designated as "GK2" in original papers (Seredenin and Gudasheva 2011; Povarnina et al. 2013)

Dispersions of gold NPs were obtained in situ by chemical reduction of Gold(III) chloride hydrate 99.999 % trace metals basis (ALDRICH, USA) using DPT or a mixture of DPT and formaldehyde (ACROS ORGANICS, A.C.S. reagent) as reducing agents in aqueous solutions in the presence of potassium carbonate. All other reagents were of analytical grade and were used as received without further purification. Double-distilled deionized water (Milli-Q (Millipore)) with resistance of 18 MΩ·cm was prepared on the day of experiment. Five different samples P1–P5 have been investigated depending on the combination and the molar ratio of components. A summary of experimental setup is shown in Table 1. The aqueous solution of DPT solution with added salt is designated as sample P1.

Synthesis of gold NPs (samples P2–P5) was performed as follows: 0.5 ml of 0.4 %wt solution of $HAuCl_4 \cdot 3H_2O$ was added to a specified volume of water under constant stirring. The mixture was heated to 95 °C for 30–40 min under intense stirring, and remaining components of the synthesis have been added sequentially: a fresh stock DPT solution, potassium carbonate and formaldehyde. All reactions gave a coloured dispersion of gold NPs: sample P2 became pink in colour, and the samples P3–P5 demonstrated a deep crimson colour, indicating that the gold ions were reduced to form Au-NPs.

The IR spectra were recorded by a Nicolet 6700 spectrometer in the transmission mode with a resolution of 2 cm^{-1} averaged over 128 scans in a wavenumber range of 3700–400 cm^{-1}. For IR measurements, thin layers of samples P1 and P2 were deposited on KRS-5 windows using a standard technique. Particle size of the

Table 1 A summary of the experimental setup and the size of gold nanoparticles

Samples	Water (ml)	The volume of 0.1 %wt DPT (ml)	The volume of 0.1 %wt K_2CO_3 (ml)	The volume of 0.37 %wt formaldehyde (ml)	$HAuCl_4$ 0.4 %wt (ml)	Particle size (nm)
P1	22.0	2.0	0.5	–	–	–
P2	22.0	2.0	0.5	–	0.5	2 peaks: 10 and 60 nm
P3	21.0	2.0	0.5	1.0	0.5	2 peaks: 2–3 and 76 nm
P4	12.5	10.0	1.0	1.0	0.5	3 peaks: 8, 100 and 600 nm
P5	18.0	5.0	1.0	0.5	0.5	one narrow peak at 34–36 nm

synthesized Au-NPs was evaluated by dynamic light scattering (DLS) by a Zetasizer Nano ZS (Malvern, UK) analyzer. It was assumed that gold NPs were spherical in shape and that chloroauric acid trihydrate and DPT reacted completely.

For the formulation of solid layers, DPT solution and synthesized Au-NP dispersions were deposited at room temperature onto various substrates: surfaces of polycrystalline gold prepared by thermal vacuum evaporation, cleaned surfaces of glass and freshly cleaved mica. The deposited layers were dried in air at room temperature. Two methods of deposition were used: drop casting technique and spin coating at 2000–3000 rpm, resulting in thin and ultrathin layers, respectively. Prepared layers showed dramatic differences not only in film thickness, but also in film structure. In the first case, a droplet of a colloid dispersion left a ring-shaped spot, the so-called "coffee ring", on a solid substrate after solvent evaporation. The maximal averaged layer thickness determined by optical microscopy and profilometry was found about 1 μm and the border line was several microns in height. For the second approach, ultrathin layers with radial thickness and without border line were obtained. Besides, in this case, one can investigate the concentration effects on both the crystallization process and final morphology of the solid layer. It is worth mentioning that the main difference between two methods consists in more equilibrium conditions of growth process and more pronounced dependence of the layer structure on the distance from the droplet centre in the case of drop casting technique. The methods used for the preparation of solid layers in present exploratory study help gather preliminary information about system design including molar ratios of components, substrates, etc. for further more complex experiments with layer height control.

The atomic force microscopy (AFM) has been used to study the morphology and microstructure of DPT and DPT/Au-NP coatings using a universal high-vacuum AFM–STM probe microscope "Solver HV-MFM" (NT-MDT, Russia) at Metrological laboratory of the State Engineering Centre of the Moscow State Technological University STANKIN. All measurements were performed at room temperature either in air or under a vacuum of 10^{-5} Pa. No significant differences in results were obtained in these two cases. Therefore, all subsequent measurements were carried out at room temperature in air.

To complement the experimental findings, a full-atomistic molecular dynamics (MD) simulation of the adsorption of an isolated DPT chain in aqueous (implicit model) solution is performed in BIOVIA Materials Studio 8.0 (BIOVIA 2014). Structural characteristics, intramolecular forces and the interactions with surfaces have been modelled within polymer consistent force field analogously to the previous simulations (Gus'kova et al. 2010). Mica (muscovite, surface area $S = 10.28$ nm^2), gold (111, surface area $S = 13.01$ nm^2) and amorphous silica (siloxane groups were saturated with hydrogen, surface area $S = 12.9$ nm^2) surfaces were considered taking into account their real chemical structure and modelled as immobile layers at the bottom (*ab* plane) of the simulation cell. The vacuum slab in *c* direction of the simulation box was kept fixed at 10 nm for every simulation setup.

Gold atoms in the simulations carried no charge; therefore, all the interactions between the adsorbate and the substrate were considered to be purely van der Waals interactions and described by Lennard-Jones potential. Molecular models of mica and silica surface have been described previously (Gus'kova et al. 2010; Guskova et al. 2013; Heinz et al. 2009). The atoms of

these surfaces carried partial charges, and the intermolecular adsorbate/adsorbent interactions included additionally Coulomb contribution (Ewald summation method). The systems in our study were simulated using molecular dynamics in an NVT ensemble. The calculations were performed at $T = 300$ K. The temperature was controlled with the Nosè–Hoover thermostat. After the equilibration phase (1 ns), the DPT conformational properties were analysed using MD trajectories of length 4 ns.

Results

Synthesis of nanocomposites and the size of gold NPs

The reaction conditions for the synthesis of NPs and nanocomposites, their stability and NPs size distributions are presented in Table 1. As follows from the experimental setup, the total volume of the reaction mixture is fixed at 24.5 ml, which means that the amount of gold is the same (ca. 0.00023 g-atom/l) in all samples. The samples P2 and P3 contain only 0.0001 g-mol DPT. In sample P4, DPT concentration is five times higher than in the previous samples (0.0005 g-mol) and two times higher than the concentration of gold in this sample.

For the sample P2, DPT acts as a reductant of gold ions. It has been demonstrated previously that PTs having amino groups in the side chains can reduce gold salts to form Au-NP without adding any reducing agent under boiling conditions (Gong et al. 2015). In our case, two amino groups of DPT chain firstly attract the oppositely charged chloroaurate anions in aqueous phase and then play a role as a mild reductant; here amides or ketones as oxidation products of the amino groups might appear, as it was obtained in a polyamine-induced gold NPs formation (Sun et al. 2006). The redox reaction for sample P2 is rather slow, and after 1 h the bimodal dispersion with average Au-NP size of 10 and 60 nm is formed. This colloidal system is characterized as unstable and aggregates within a month.

When strong reducing agent formaldehyde is added to the mixture with the same ratio of the reactants (sample P3), the Au-NP dispersion is formed rapidly within 10–15 min. However, in this case, we also obtain an unstable system with a bimodal particle size distribution. It comprises smaller and larger particles with an average diameter of 2–3 and 76 nm, respectively. As in previous experiment, the sample P3 aggregates within 1 month.

Sample P4 is characterized by maximal amount of DPT in the reaction mixture (Table 1). The size distribution has three peaks at 8, 100 and 600 nm. The sample is also unstable, and two values of 100 and 600 nm correspond to particles aggregates.

The most stable dispersion with a narrow monomodal particle size distribution is obtained only for sample P5 with 1:1 molar ratio of components (Table 1). This system is classified as the most stable for a prolonged period of time (more than 3 years' storage at room temperature).

In samples P3–P5, DPT can adsorb on the gold surface during the synthesis (Bhargava et al. 2005; Selvakannan et al. 2004; Aryal et al. 2006; Negishi and Tsukuda 2003; Wu et al. 2015) preventing them from aggregation or in the last stages of Au-NP nucleation and further growth probably via ligand substitution reaction. In any case, the surface of gold NP exhibits a high affinity for the amino groups of DPT (Horovitz et al. 2007; Zakaria et al. 2013) giving rise to various bioconjugates.

It is worth noting that DPT itself can undergo modifications in mixtures with formaldehyde. Usually such reactions involve N-terminal groups and side amino groups of lysine (Metz et al. 2004) forming methylol groups or Schiff bases. Further investigations are required to identify the formaldehyde-induced DPT alteration.

Thus, the component composition for the synthesis of highly stable gold colloidal dispersion in DPT/formaldehyde solution is formulated (Sample P5). It is shown that DPT itself can function as a reductive agent of gold ions (Sample P2). The latter provides a convenient system for investigating the Au-NP/DPT interactions in bioconjugates using IR spectroscopy.

IR spectroscopic studies of Au-NP/DPT bioconjugates

In order to understand the character of binding in Au-NP/DPT conjugates at the molecular level, and to study how NPs affect the conformation and the self-assembly of DPT which finally reflects in morphological changes of functional PT composites, IR spectroscopy has been applied. As reference systems, IR

spectra of two peptide solutions are recorded: the first one corresponds to the solution of pure DPT at pH 4 (Fig. 2, spectrum *1*), and the second one is the sample P1 (Fig. 1, spectrum *2*).

These two cases are considered with the aim to characterize the influence of pH on the chain conformation. The spectrum of the Au-NP/DPT bioconjugate (sample P 2) is depicted as well (Fig. 2, spectrum *3*). Assignment of IR bands of DPT is performed on the basis of the data available in the literature (Philip 2009; Basavaraja et al. 2008; Ahmad et al. 2003; Venyaminov and Kalnin 1990).

The stretching vibrations of the NH groups have several absorption bands in the region of 3500–3000 cm^{-1} in spectra *1* and *2*. Indeed, this stretching appears as a doublet of two broad absorption bands at 3292 and 3074 cm^{-1}, which corresponds to vibrations of hydrogen-bonded NH groups. Some authors (Miyazawa 1960) consider the low frequency band of this doublet as an overtone of the Amide II vibration for the trans-configuration of the amide group of secondary amides. A barely visible shoulder on the high-frequency band at 3292 cm^{-1} corresponds to the stretching vibrations modes of the hydroxyl end groups of DPT connected via hydrogen bonds. In the region of the Amide I and Amide II bands, the most intense absorption of DPT is observed (spectrum *1*). It is interesting to note that both bands have a complex contour, almost the same intensity and are symmetric with respect to each other. The position of two amide bands provides the information about the conformational states and alterations in the secondary structure of the PT (Dong et al. 1990). In the present case, these bands form symmetric doublet characterizing α and β conformation of the DPT molecule. The band at 1547 cm^{-1} (Amide II) clearly indicates the trans-configuration of the peptide groups in the DPT molecule. The carbonyl band (ν_{ass}) at 1655 cm^{-1} (Amide I) has a shoulder at 1720 cm^{-1}, which points out that not all terminal carboxyl groups are ionized in DPT molecule. Symmetric oscillations (ν_{ss}) of the ionized carboxyl groups correspond to the band at 1409 cm^{-1}. In the region of 1300–1130 cm^{-1}, a broad absorption band with maxima at 1174, 1252 and 1304 cm^{-1} is observed. It corresponds to in-plane bending vibrations of CH and NH bonds (Amide III). Thus, IR results demonstrate that DPT molecules are strongly intermolecularly hydrogen bonded in the solid state at pH 4.

As one would expect that upon thermal DPT treatment and in the presence of added salt (pH 7), IR absorption spectrum undergoes a remarkable change (Fig. 2, spectrum *2*). At this pH, all the carboxyl groups are ionized and as a result, the absorption band at 1720 cm^{-1} of non-ionized COOH groups disappears. The band at 1622 cm^{-1} and a sharp shoulder near 1649 cm^{-1} correspond to ionized carboxyl groups. Therefore, the ionized terminal groups and PT groups (Amide I) are now better resolved in the spectrum, and the latter band is shifted towards lower frequencies by 32 cm^{-1}. Besides, all characteristic PT bands become very intense: the band intensity ratio of Amide I to the stretching vibrations band of CH group equals 2.9 (spectrum *1*) and 5.9 (spectrum *2*), and the band intensity ratio of Amide III to the stretching vibrations band of CH group is 1.3 (spectrum *1*) and 10 (spectrum *2*). Both the significant increase in band intensities and the shift of Amide I band towards lower frequencies might be attributed to the changes in DPT chain packaging from β-antiparallel to β-parallel structure in the folded layer. Shift of absorption band occurring as a result of structural changes leads to the appearance of two new IR bands centred at 1009 and 836 cm^{-1} (spectrum *2*) are attributed to the ν_4 bending vibrations of NH group in the plane of the amide group and to ν_5 skeletal modes of N–C and C–C bonds, respectively. A weak absorption band at 1397 cm^{-1} corresponds to the absorption of potassium carbonate.

The IR spectrum of DPT/Au-NP bioconjugate is presented in Fig. 2 (spectrum *3*). Assuming that DPT acts as gold reductant and amine groups of Lys are participating in this redox reaction, the corresponding bands of amino groups in spectrum *3* should be less intense as compared to the bands in spectrum of DPT (spectrum *2*). Indeed, the NH stretches at 3300 and 3074 cm^{-1}, which are clearly seen in the spectra *1* and *2*, are almost negligible in the spectrum *3* because of broad absorption bands of hydrogen-bonded NH and OH groups in region. When comparing spectra *3* and *2*, one can conclude that Amide I and Amide II differ significantly. For instance, the absorption bands of ionized carboxyl groups become very broad and have a complex contour, which is an indication of partially overlapping bands. A new band appears at 1649 cm^{-1} (spectrum *3*), which was previously detected as a shoulder of Amide I band at 1622 cm^{-1} (spectrum *2*). All these data suggest that PT in the sample P2 has more than two types of ionized carboxyl groups,

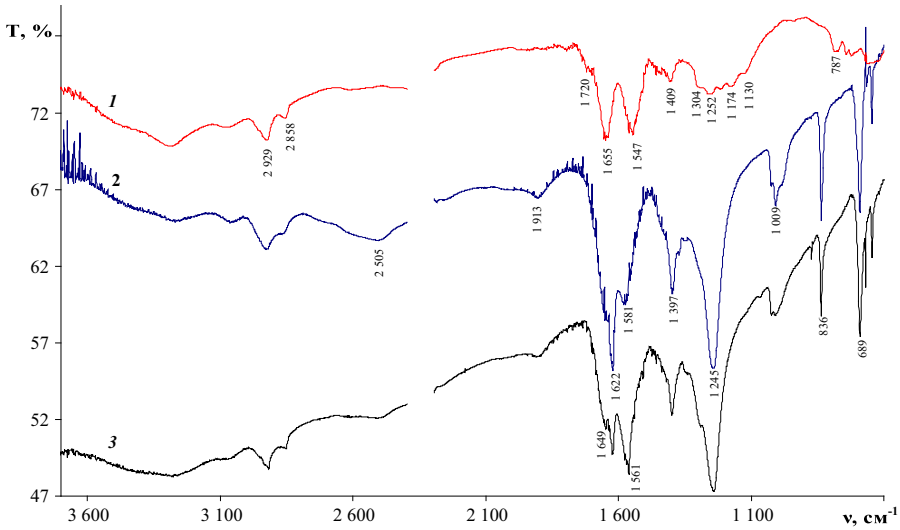

Fig. 2 IR spectra of DPT at pH 4 (*1*), sample P1 at pH 7 (*2*) and sample P2 at pH 7 (*3*)

meaning that ionized carboxyl group of the PT form various bonds/compounds with Au-NP, e.g. monodentate, bidentate-cyclic, bidentate-bridged complexes, etc. The appearance of a shoulder at 1265 cm^{-1} on the intensive Amide III band is also associated with a specific interaction between the carboxyl group and gold NP. Similar IR absorbance band has been observed in Au-NP dispersion produced by a reduction of $HAuCl_4 \cdot 3H_2O$ by cellulose derivatives as an indication of bioconjugation (Urupina et al. 2013). The most intensive bands in spectrum *3* correspond to in-plane NH bending and changes of CNH angles (for the comparison, in spectrum *2* the carbonyl band at 1622 cm^{-1} (Amide I) is the most pronounced one). It confirms the structural changes of DPT molecules in the process of formation of bioconjugates define which groups of DPT take part in formation of the Au-NPs conjugated complexes and show that Au-NPs affect the self-assembly motifs of PTs in thin films.

The structure of thin and ultrathin layers

Morphological characterisation of DPT films at different pH

In order to obtain insight about the morphology of the DPT thin films and DPT/Au-NPs nanoarchitectonics, atomic force microscopic measurements were carried out. Figure 3 shows the AFM images of thin and ultrathin DPT layers deposited at pH 4 (i.e. at the isoelectric point of the DPT) on mica and glass surfaces. These samples correspond to the spectrum *1* in Fig. 2. In the case of ultrathin layer at 1:30 dilution (Fig. 3a), a structureless layer forms with a surface roughness of 0.5–1 nm.

The morphology of thin layers of DPT on the glass surface can be characterized as having elongated short chains formed by individual flat particles ("pancakes") as main structural elements of self-assembling (Fig. 3b, lower left corner). These building blocks form 100-μm-long chains composed of individual flat particles with an average length of ca. 800 nm, a width of 1.2 mm and a height of 100–150 nm. For the latter, the aspect ratio length/width is 2/3. The longer chains are built atop of the layer consisting of tightly packed "pancakes" which can be seen at higher resolutions. Their average size is ca. 50 nm and the aspect ratio height/diameter is 1/10. On the surface of mica, DPT forms separated 3D islands which then coalesce (Fig. 3c).

Figure 4a shows the AFM image of ultrathin DPT layer at pH 7 on mica (this system corresponds to spectrum *2*, Fig. 2). According to IR results, when pH increases, the structure of DPT undergoes significant changes. These alterations related to the changes of the DPT total charge induce molecular self-assembly and the generation of more crystalline films which consist of narrow plates having width of 200–300 nm and height of ca. 0.5 nm. Over this structural layer, the growth of flat isolated particles further proceeds. At pH 10 on glass substrate, DPT chains build dendritic structures atop of a continuous peptide layer (Fig. 4b).

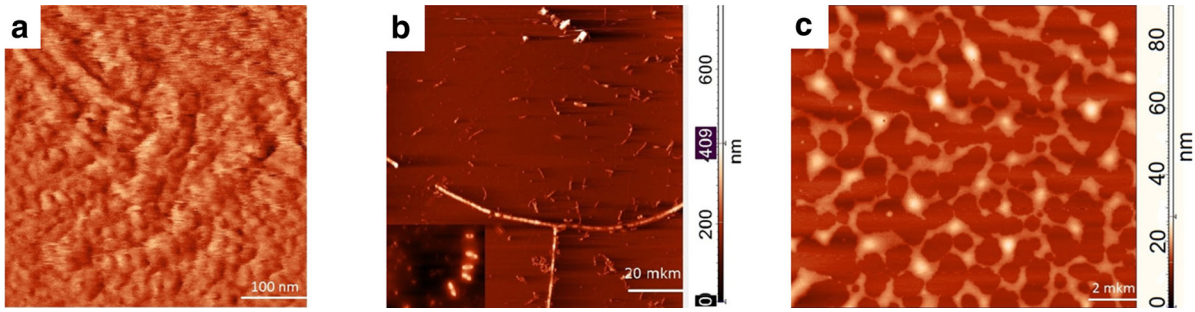

Fig. 3 AFM image of DPT-based layers; ultrathin layer (1:30 dilution) on mica (phase image) (**a**) and thin layers without dilution on glass (**b**) and mica (**c**)

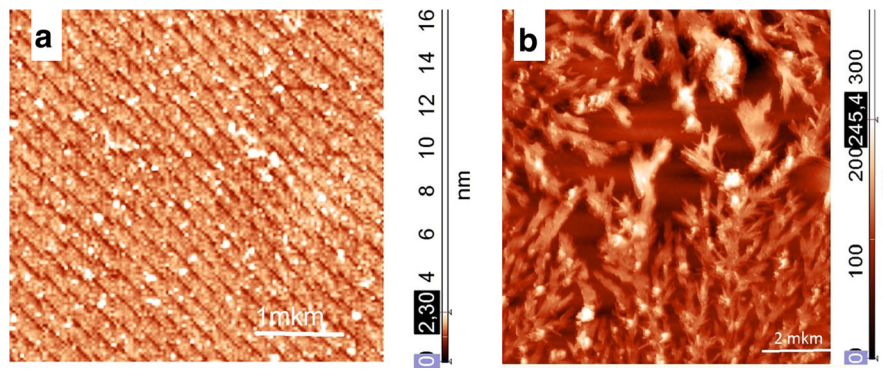

Fig. 4 AFM images of dipeptide layers (Sample P1); ultrathin layer (pH 7, 1:30 dilution) on mica (**a**) and thin layer without dilution at pH 10 on glass (**b**)

The angle between the branches of dendrites is 30–40°. The formation of such structures was never observed at pH 4 (Fig. 3b).

When the concentration of DPT in solution increases (pH 7, 1:10 dilution), the individual mesocrystals are growing on mica (Fig. 5). Their height is less than 80 nm, and the angles formed by the crystal faces are 60° and 120°. These structural features indicate on one side a higher degree of perfection of such mesocrystals and on the other side, that the growth front is formed by certain crystal facets. Along with mesocrystals, the chain-like aggregates are observed on the mica surface. Their structure is similar to the structure of DPT layers at pH 4 in Fig. 3. The height of these chains does not exceed 4 nm.

Morphological characterisation of Au-NPs/DPT conjugates

Figure 6 shows the first example of DPT composite layers with gold NPs, which corresponds to the IR experiment on Fig. 2 (spectrum *3*). As it was outlined above, for sample P2, DPT plays a dual role as a reductant of gold ions and as a stabilizer of NP surface. In this case, we also see the formation of dendrites and the dendrite-like structures on top of a layer of separated particles. However, unlike the dendrites depicted in Fig. 4b, the angle between the branches in composites is 90°.

Figures 7, 8 and 9 illustrate the morphologies of DPT/Au-NPs composites synthesized with formaldehyde as reducing agent at various molar ratios of DPT. The most dramatic structural changes occur in these samples (P3–P5, Table 1).

Figure 7 shows the AFM images of a composite layer prepared with gold excess as compared to the amount of DPT in the reaction mixture. Along with dendrites whose structure was obtained to be similar to depicted one in Fig. 6, the formation of various cubic-shaped mesocrystals is observed (Fig. 7a). The cube sides reach 10–15 μm (Fig. 7c). However, their height does not exceed 0.5 μm. Two structural features are important to note: first of all, such mesocrystals are characterized by the presence of the cavity having four-sided inverted pyramid shape and located at the

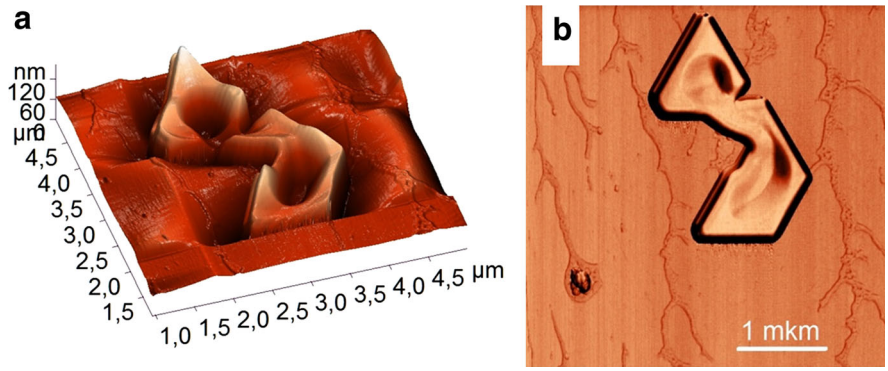

Fig. 5 AFM image of DPT mesocrystal after deposition of ultrathin dipeptide layer (pH 7, 1:10 dilution) on mica; 3D image (**a**) and phase image (**b**)

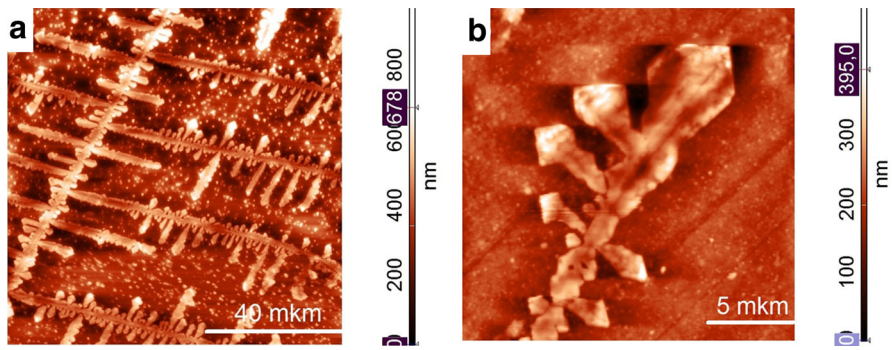

Fig. 6 Self-assembly and fractal feature of thin layers of DPT/Au-NPs (Sample P2) on glass (**a**) and gold (**b**). (Color figure online)

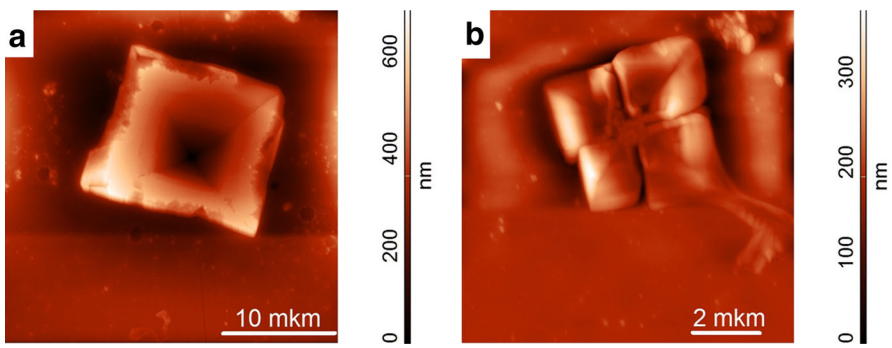

Fig. 7 AFM image of different mesocrystals in thin layers of DPT/Au-NPs (sample P3) on glass surface

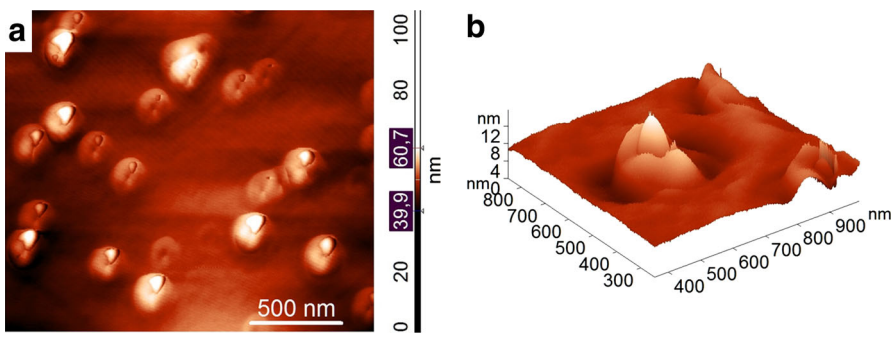

Fig. 8 AFM image of Janus particles in thin layers of DPT/Au-NPs (sample P3) on glass: Janus particles (**a**), a detailed 3D image of Janus particle (**b**)

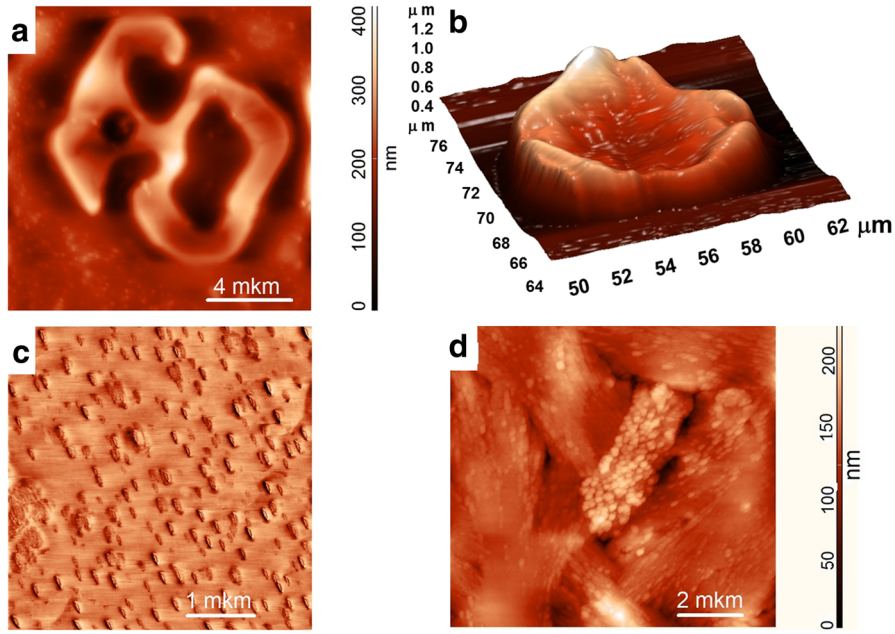

Fig. 9 AFM images of different areas on the surface of thin layers of DPT/Au-NPs (sample P4) (**a**,**b**), lateral forces image (**c**) deposited on a glass substrate (**a**–**c**) and gold (**d**). (Color figure online)

centre of the cube; secondly, the formation of different twins is detected as well (Fig. 7b). Twin crystals were also detected earlier in other experiments on synthesis of composites based on plate-like gold monocrystals and PTs (Brown et al. 2000; Kim et al. 2010).

Another interesting morphology seen in thin layers of sample P3 is the growth of Janus-like particles (Fig. 8), which is detected only for such molar ratios of components. Their analysis reveals that all these particles have the same geometry and structure, which indicates their fractal nature. They are sufficiently flat in shape: the aspect ratio height/diameter does not exceed 1/10 and does not change substantially from particle to particle. Phase contrast imaging does not detect significant differences between Janus particles and the surface layer. This may be an indirect indication that the upper part of Janus particles (Fig. 8b) is also covered with DPT layer.

The sample P4 is prepared with both DPT and potassium carbonate excess in solution as compared to gold content. In this case, the growth of mesocrystals with different shapes is also seen (Fig. 9). A characteristic feature of all of these structures is the presence of the cavity at their centre. Similar to the previous case (Fig. 7), three-dimensional mesocrystals are also formed (Fig. 9a,b). However, they have more diverse shapes and are more disordered. The glass surface between mesocrystals is not covered with DPT layers. In other areas of the glass surface, various aggregates or clusters are present. They are oriented in a certain direction on the surface and consist of ordered linear chains of 3–4 separated NPs (Fig. 9c). The size of NP is 40–50 nm, and the aspect ratio height/diameter is of 0.1–0.2. The formation of such aggregates is a result of the self-assembly of Au-NPs. Similar aggregates of NPs are formed on the surface of gold (Fig. 9d). But in this case, they form dense layers without preferable orientation.

The sample P5 represents the most stable dispersion of DPT/Au-NPs. The ultrathin layers of P5 are shown in Fig. 10a. The layers consist of gold NPs immersed in the DPT matrix. The thickness of the layer is negligible as evidenced by the presence of small pores. The average NP size is 50 nm and the height is less than 2 nm which results in the aspect ratio of 0.04. These data show that gold NPs have a shape of very thin flat discs, rather than spheres. Thin layers on the glass substrate are characterized by the regions which contain only self-assembled gold NPs (Fig. 10b) and dendrites, similar to those shown in Fig. 6. The size of gold NPs (Fig. 10b) is 60–70 nm with aspect ratio of 0.2. The processes of NPs self-assembly lead to the formation of elongated aggregates, oriented along a certain direction. Such ordering of the NPs is also observed in the case of sample P4 (Fig. 9c). It is worth mentioning that the self-assembling of gold NPs is

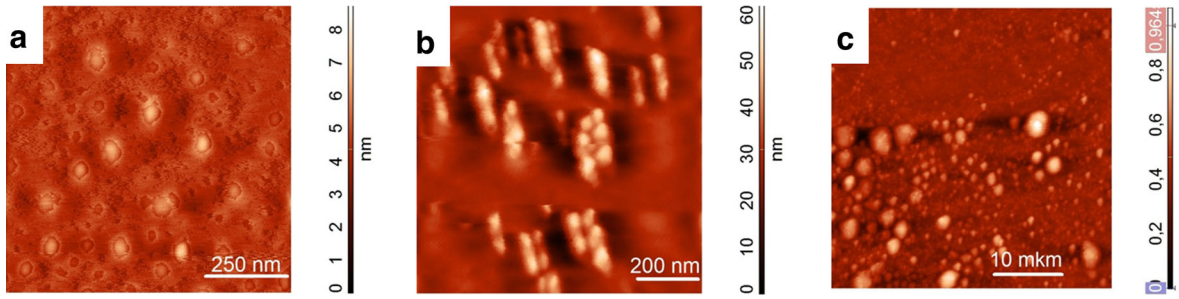

Fig. 10 Ultrathin layers of DPT/Au-NPs (sample P5, 1:10 dilution) on mica (**a**) and thin layers without dilution on glass (**b**) and gold (**c**). (Color figure online)

observed only in samples P4 and P5, and that mesocrystals were never observed in sample P5. Only disordered structures consisting of individual flat particles of different sizes are observed on the gold substrate (Fig. 10c). The reason for these differences may be explained by higher concentrations of reagents in sample P4. These data indicate the determining role of reactant molar ratios in the processes of molecular self-assembly of gold NPs.

Dipeptide self-organization: test molecular dynamics simulations

In order to summarize the experimental results described in the previous sections and to shed light on possible mechanisms of nanostructure formation, it is necessary to consider the properties of an isolated DPT chain and its interactions with gold, mica and silica surfaces.

The total charge of DPT molecule depends on pH, because it contains amino acids with ionic side groups, which can strongly interact with charged surfaces of adsorbents (Rimola et al. 2013). The presence of charged groups of DPT upon pH changes is confirmed by IR measurements (Fig. 2). The total charge Q of DPT in the absence of intramolecular interactions between the functional groups can be estimated using Henderson–Hasselbalch equation (Fig. 11a). This Figure (Fig. 11b,c) depicts the snapshots of the neutral and negatively charged DPT molecule in its optimized geometry as well. From the picture follows that in a strongly acidic environment, the total charge is positive and is equal $+2$, which corresponds to two protonated amino groups of lysine. Molecule is neutral when pH reaches the value of 3 and is characterized by four stabilizing intramolecular hydrogen bonds, which are shown in Fig. 11b. At pH > 5, DPT becomes negatively charged due to the acid dissociation of two terminal carboxylic groups at first, and then at pH > 10, Q reaches the value -4 due to the acid dissociation of two carboxylic groups at the side chains of the glutamic acid residues. Conformation of an isolated anion in a strongly basic environment is stabilized by eight intramolecular hydrogen bonds. Because of the repulsion of like-charged groups, the DPT chain stretches and its radius of gyration increases.

A majority of experiments on nanocomposite synthesis are conducted at pH 7, which corresponds to DPT molecule having one or two ionized terminal carboxyl groups; and two uncharged amino groups of lysine residues can participate in coordination with gold NP surface. Transition from pH 4 to 7 promotes the growth of a number of ionized carboxylic groups and the conformational changes, which are in agreement with IR spectra (Fig. 2).

The aggregation of NPs into anisotropic chain-like structures proceeds probably according to the mechanism of bridge formation between adjacent NPs. If we consider DPT molecule in its elongated conformation, then we can assume that amino groups are connected covalently or ionically to the surfaces of two adjacent NPs, or both amino groups are attached to one NP and the aggregate is stabilized via hydrogen bonding between carboxylic groups of two DPT chains on two NPs next to each other. Thus, such a combination of Lys and Glu residues governs the unique properties of DPT: lysine coordinates with NPs, and glutamic acid, which itself acts as stabilizer of NPs (Zakaria et al. 2013), in combination with lysine can promote directional growth of aggregates via non-covalent interparticle interactions.

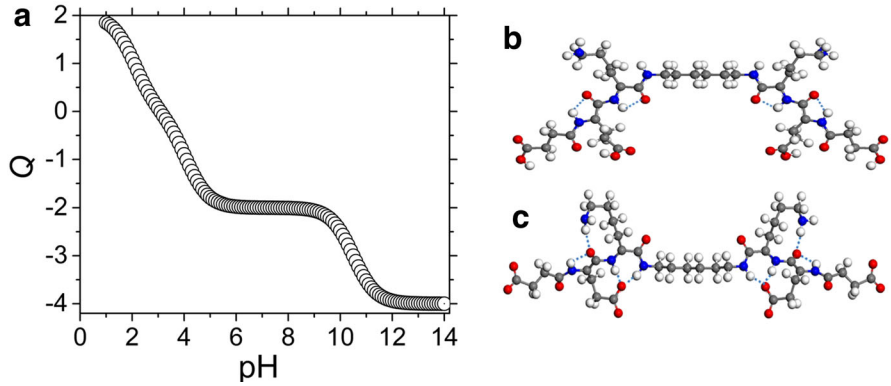

Fig. 11 Total charge of the DPT as a function of pH calculated using Henderson–Hasselbalch equation (**a**) and the conformations of neutral molecule (**b**) and molecular anion at $Q = -4$ (pH > 12) (**c**). Optimization of molecular geometry is performed using density functional theory at B3LYP/6-31G(d,p) in Gaussian 09 (Rev. A01) (Frisch et al. 2009). Carbon, oxygen, nitrogen and hydrogen atoms are coloured *in grey, red, blue* and *white*, respectively. Intramolecular hydrogen bonds are shown as *light-blue dashed lines*. (Color figure online)

The strong dependence of the morphology of DPT layers on the nature and roughness of the adsorbent surface indicates a significant role of interfacial interactions in the NPs growth and self-assembly processes. This dependence is clearly seen in the case of ultrathin DPT layers growing on the surface of freshly cleaved mica, which is the most active one among considered substrates (Fig. 12a).

We have previously found out that Au-NPs self-organization in composite layers based on cellulose derivatives (Urupina et al. 2013) and more complex peptides consisting of seven amino acids (Loskutov et al. 2015) is observed in case of weak particle/substrate interactions at poor wetting conditions and at low rate of solvent evaporation. Apparently, the stronger interactions between negatively charged carboxyl groups of DPT and positively charged mica surface due to a large number of potassium ions prevent the formation of extended ordered structures.

Strictly speaking, DPT molecule (Fig. 1) belongs to a class of diantennary peptides (Gus'kova et al. 2010), since two PT fragments in its structure are separated by a short alkyl (hexyl) hydrophobic spacer. Owing to amphiphilic character of the molecule, i.e. the combination of polar, water-soluble PT antennas and hydrophobic hydrocarbon chain, DPT chain self-organizes differently on the substrates of various polarities. Figure 12 illustrates the behaviour of the molecule at pH 7, when two terminal carboxylic groups are negatively charged. These groups of two antennas are anchored on mica surface through hydrogen bonding and electrostatically (Fig. 12a). Similar behaviour of carboxylic group of model tripeptide H–Lys–Glu–Lys–NH_2 on mica was described by Monti et al. (Monti et al. 2009). Remaining part of the molecule including its central hydrophobic unit stays non-adsorbed due to the high surface charge of muscovite. Therefore, anchored DPT chains are ordered parallel to mica surface, and strongly interact with the substrate.

On the non-charged surface of gold DPT chain adsorbs entirely (Fig. 12b). Here COOH and NH_2 groups build intramolecular hydrogen bonds. Because of the van der Waals character of the interaction between the chain and the surface, the strength of the adsorption is moderate. The silanol SiOH groups on the silica surface can participate in hydrogen bonding with PT chains. Because of the surface roughness, molecules are found to be tilted with respect to the surface (Fig. 12c). The interaction between molecules is weak hydrogen bonding between amino- and carboxylic groups and silanol groups of the silica, which is confirmed by quantum chemical (Rimola et al. 2009) and molecular dynamics simulations (Laura Gambino et al. 2006) of Lys and Glu adsorption onto silica.

During solvent evaporation, the cocrystallization of all components of a colloidal solution is likely to occur. The solvent contains Au-NPs functionalized/stabilized with residues of formic acid or DPT, free DPT with ionized carboxyl groups (Fig. 11a) and inorganic salts. In this case, the cocrystallization may

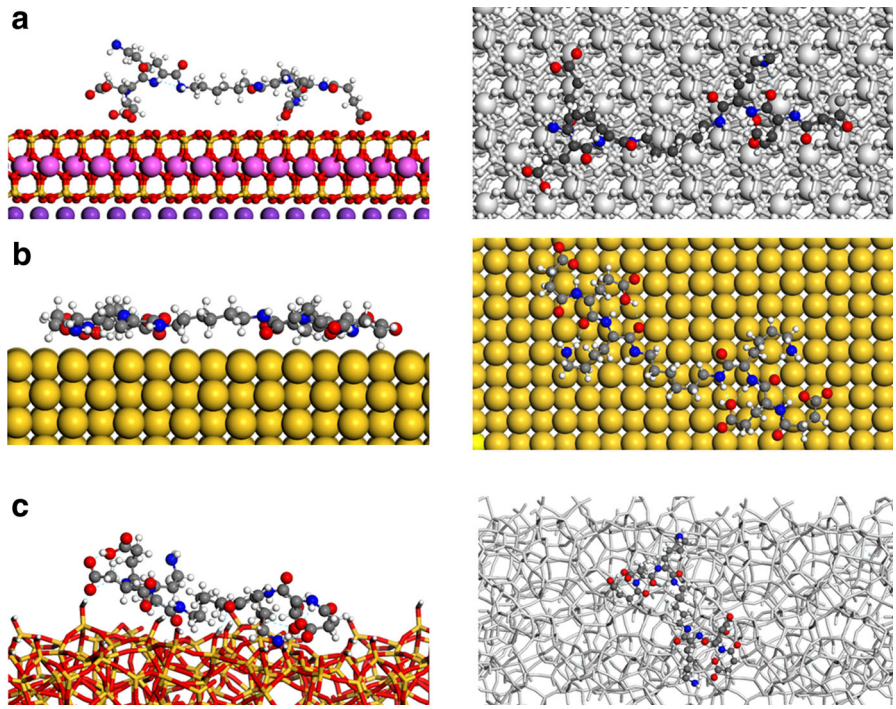

Fig. 12 Orientation of DPT molecule in the vicinity of mica (**a**), gold (**b**) and silica (**c**); side view (*left*) and top view (*right column*). Snapshots show the most energetically favourable conformation and orientation of DPT. For **a** and **c** (top views) the substrate atoms are shown in *grey* for clarity. Hydrogen bonds are shown as *blue dashed line*. (Color figure online)

occur by various mechanisms, including the non-classical crystallization with gold NPs and colloidal crystal growth (Grzybowski 2014; Bahrig et al. 2014). This may explain a wide variety of morphologies observed in the experiments and their substantial changes by varying the molar ratios of reactants or pH, which is in line with previous experimental and theoretical results (Han et al. 2013; Rusin et al. 2013; Losev et al. 2013).

Discussion of the results

The presence of Au-NPs affects both self-assembly/growth of the DPT layers and finally the morphology of nanostructures in several ways. For instance, Au-NPs create a number of crystallization centres. This causes the formation of structures consisting of flat particles. The NPs play a role of obstacles to the directional growth of DPT assemblies. Bioconjugation of DPT to the surface of gold NP can alter or even prevent the formation of ordered structures: the crystallinity of DPT layers is lowered and the diversity of their morphology is reduced as compared to the sample P1. As it was outlined above, for highly branched DPT/Au-NPs dendrites (Fig. 6), the angle between the direction of the growth of the main and side branches is 90°. This is a typical value for the diffusion-limited crystallization of polymers, in which the crystal growth rate is determined by the diffusion rate of macromolecules from the liquid phase to the crystal growth front and the probability of chain attachment to the different parts of the front is almost the same (Wang et al. 2004).

Our experimental results demonstrate that the structure and morphology of the thin layers of the DPT composite depend significantly on the properties of the substrate–layer interface. Otherwise, on different substrates, we would observe the same morphology of relatively thick layers. The crystallization processes are largely dependent not only on the nature of the substrate, but also on the surface roughness and the method of deposition used. As a consequence, at different areas of the same substrate, the various structures can be observed. This is important especially in the case of thin layers formation by drop casting technique. In general, evaporating droplet of a colloidal solution deposited on a solid surface is a complex non-equilibrium system, where the supersaturation is constantly changing; there are gradients of concentration, temperature, and the mass transfer from the centre of the droplet to its borders. Therefore, the thin layer structure formed at the centre and at the rim

of the droplets can vary significantly. Besides, the final morphology depends upon NPs size and the local concentration of components, the overall geometry and surface pattern of the NPs (Alfimov et al. 2006).

The aspect ratio height/diameter of gold NPs is found in the range of 0.1–0.2 which indicates a disc-like shape rather than a spherical particle. NPs with similar geometric characteristics have been synthesized earlier by Brown et al. (Brown et al. 2000) in the reduction of gold ions by other peptides promoting the growth of metal crystals in a specific direction, as well as in our previous studies (Loskutov et al. 2015). It should be emphasized that DLS method based on Mie scattering, a priori assumes a spherical particle shape. In our case, the particles have a disc-like shape. Therefore, the numbers collected in the Table 1 may not correspond to the real geometrical dimensions of nanoparticles. In order to improve this situation, the multiangle light scattering should be applied, which is beyond that allowed by our standard equipment .

Obtained cubic mesocrystals (Fig. 7) have well-faceted pyramidal cavity at the centre. Previously, it has been suggested (Losev et al. 2013) that such unique crystal faces are chemically active and may serve as active centres for the adsorption of DPT molecules. Observed twin structures have been found in other experiments with plate-like single crystals of Au-NPs in nanocomposites with various PTs (Brown et al. 2000; Kim et al. 2010). Janus particles depicted in Fig. 8 can be considered as components for the formulation of more complex superstructures (Walther and Müller 2013; Jiang et al. 2012). This enables a fine-tuning of their shape, which in addition to their anisotropic structure leads to the development of new properties (Liang et al. 2014).

Conclusions

In this work, an approach to formulate PT composite layers with gold NPs through in situ reduction of chloroauric acid trihydrate by DPT and/or DPT/formaldehyde mixture in the presence of potassium carbonate is proposed. Spectroscopic measurements suggested that DPT acts as a mild reductant of gold and builds bioconjugates with Au-NPs surface stabilizing them in colloidal solution. At the same time, the self-assembly of DPT chains on solid surfaces is affected by gold NPs and accompanied by changing PT chain conformations. The morphological properties of solid layers are investigated by AFM measurements. As a result, a diverse set of crystal morphologies is observed including disc-like particles, dendrites, chains, mesocrystals, and Janus particles. It is shown that the morphology of PT-based thin films or DPT/Au-NP nanoarchitectonics substantially depends on the molar ratio of the components, pH, the substrate chemistry and topology, and the deposition technique. We believe that our results would allow for further development of various PT/NPs nanocomposites with prescribed properties. The approaches used in this work to form DPT/Au-NPs nanoarchitectonics may be useful for the formulation of a variety of nanostructures for practical applications in biomedical, electronic, and nanotechnological fields of modern materials science.

Acknowledgments This study was supported by the Ministry of Education and Science of the Russian Federation and by financial support from Russian Foundation for Basic Research, contract No. 15-07-01733.

References

Ahmad A, Senapathi S, Khan MI, Kumar R, Sastry M (2003) Extracellular biosynthesis of monodisperse gold nanoparticles by a novel extremophilic actinomycete, *Thermomonospora* sp. Langmuir 19:3550–3553. doi:10.1021/la026772l

Alfimov MV, Kadushnikov RM, Shturkin NA, Alievsky VM, Lebedev-Stepanov PV (2006) Imitative simulation of the processes of self-organization of nanoparticles. Ross Nanotecknol (Rus) 1:127–133

Ariga K, Li J, Fei J, Ji Q, Hill JP (2016) Nanoarchitectonics for dynamic functional materials from atomic-/molecular-level manipulation to macroscopic action. Adv Mater 28:1251–1286. doi:10.1002/adma.201502545

Aryal S, Remant Bahadur KC, Bhattarai N, Kim CK, Kim HY (2006) Study of electrolyte induced aggregation of gold nanoparticles capped by amino acids. J Colloid Interface Sci 299:191–197. doi:10.1016/j.jcis.2006.01.045

Bahrig L, Hickey SG, Eychmüller A (2014) Mesocrystalline materials and the involvement of oriented attachment—a review. CrystEngComm 16:9408–9424. doi:10.1039/C4CE00882K

Basavaraja S, Balaji SD, Lagashetty A, Rajasab AH, Venkataraman A (2008) Extracellular biosynthesis of silver nanoparticles using the fungus Fusarium semitectum. Mater Res Bull 43:1164–1170. doi:10.1016/j.materresbull.2007.06.020

Bedford NM, Hughes ZE, Tang Z, Li Y, Briggs BD, Ren Y, Swihart MT, Petkov VG, Naik RR, Knecht MR, Walsh TR (2016) Sequence-dependent structure/function relationships of catalytic peptide-enabled gold nanoparticles

generated under ambient synthetic conditions. J Am Chem Soc 138:540–548. doi:10.1021/jacs.5b09529

Bhargava SK, Booth JM, Agrawal S, Coloe P, Kar G (2005) Gold nanoparticle formation during bromoaurate reduction by amino acids. Langmuir 21:5949–5956. doi:10.1021/la050283e

BIOVIA Materials Studio (2014) version 8.0, BIOVIA, San Diego, CA, USA

Brorsson AC, Kumita JR, MacLeod I, Bolognesi B, Speretta E, Luheshi LM, Knowles TPJ, Dobson CM, Crowther DC (2010) Methods and models in neurodegenerative and systemic protein aggregation diseases. Front Biosci 15:373–396. doi:10.2741/3626

Brown S, Sarikaya M, Johnson E (2000) A genetic analysis of crystal growth. J Mol Biol 299:725–735. doi:10.1006/jmbi.2000.3682

Conejero-Muriel M, Contreras-Montoya R, Díaz-Mochón JJ, de Cienfuegos LÁ, Gavira JA (2015) Protein crystallization in short-peptide supramolecular hydrogels: a versatile strategy towards biotechnological composite materials. CrystEngComm 17:8072–8078. doi:10.1039/C5CE00850F

Dahl JA, Maddux BLS, Hutchison JE (2007) Toward greener nanosynthesis. Chem Rev 107:2228–2269. doi:10.1021/cr050943k

Dong A, Huang P, Caughey WS (1990) Protein secondary structures in water from second-derivative amide I infrared spectra. Biochemistry 29:3303–3308. doi:10.1021/bi00465a022

Frisch MJ, Trucks GW, Schlegel HB, Scuseria GE, Robb MA, Cheeseman JR, Scalmani G, Barone V, Mennucci B, Petersson GA, Nakatsuji H, Caricato M, Li X, Hratchian HP, Izmaylov AF, Bloino J, Zheng G, Sonnenberg JL, Hada M, Ehara M, Toyota K, Fukuda R, Hasegawa J, Ishida M, Nakajima T, Honda Y, Kitao O, Nakai H, Vreven T, Montgomery JA Jr, Peralta JE, Ogliaro F, Bearpark M, Heyd JJ, Brothers E, Kudin KN, Staroverov VN, Kobayashi R, Normand J, Raghavachari K, Rendell A, Burant JC, Iyengar SS, Tomasi J, Cossi M, Rega N, Millam JM, Klene M, Knox JE, Cross JB, Bakken V, Adamo C, Jaramillo J, Gomperts R, Stratmann RE, Yazyev O, Austin AJ, Cammi R, Pomelli C, Ochterski JW, Martin RL, Morokuma K, Zakrzewski VG, Voth GA, Salvador P, Dannenberg JJ, Dapprich S, Daniels AD, Farkas Ö, Foresman JB, Ortiz JV, Cioslowski J, Fox DJ (2009) Gaussian 09, Revision A.01. Gaussian, Inc., Wallingford CT

Gong Y, Chen X, Lu Y, Yang W (2015) Self-assembled dipeptide-gold nanoparticle hybrid spheres for highly sensitive amperometric hydrogen peroxide biosensors. Biosens Bioelectron 66:392–398. doi:10.1016/j.bios.2014.11.029

Grzybowski BA (2014) Charged nanoparticles crystallizing and controlling crystallization: from coatings to nanoparticle surfactants to chemical amplifiers. CrystEngComm 16:9368–9380. doi:10.1039/C4CE00689E

Gus'kova OA, Khalatur PG, Khokhlov AR, Chinarev AA, Tsygankova SV, Bovin NV (2010) Surface structures of oligoglycines: a molecular dynamics simulation. Rus J Bioorg Chem 36:574–580. doi:10.1134/S1068162010050043

Guskova O, Schünemann C, Eichhorn K-J, Walzer K, Levichkova M, Grundmann S, Sommer J-U (2013) Light absorption in organic thin films: importance of oriented molecules. J Phys Chem C 117:17285–17293. doi:10.1021/jp4048083

Han G, Thirunahari S, Shan Chow P, Tan RBH (2013) Resolving the longstanding riddle of pH-dependent outcome of glycine polymorphic nucleation. CrystEngComm 15:1218–1224. doi:10.1039/C2CE26594J

Heinz H, Farmer BL, Pandey RB, Slocik JM, Patnaik SS, Pachter R, Naik RR (2009) Nature of molecular interactions of peptides with gold, palladium, and Pd–Au bimetal surfaces in aqueous solution. J Am Chem Soc 131:9704–9714. doi:10.1021/ja900531f

Horovitz O, Mocanu A, Tomoaia G, Bobos L, Dubert D, Daian I, Yusanis T, Tomoaia-Cotisel M (2007) Lysine mediated assembly of gold nanoparticles. Stud Univ Babes Bolyai Chem 52:97–108

Jiang S, Granick S, Schneider HJ (2012) Janus particles synthesis, self-assembly and applications. RSC, London

Karki I, Wang H, Geise NR, Wilson BW, Lewis JP, Gullion T (2015) Tripeptides on gold nanoparticles: structural differences between two reverse sequences as determined by solid-state NMR and DFT calculations. J Phys Chem B 119:11998–12006. doi:10.1021/acs.jpcb.5b04299

Kim J, Rheem Y, Yoo B, Chong Y, Bozhilov KN, Kim D, Sadowsky MI, Hur H-G, Myung NV (2010) Peptide-mediated shape-and size-tunable synthesis of gold nanostructures. Acta Biomater 6:2681–2689. doi:10.1016/j.actbio.2010.01.019

Knowles TPJ, Buehler MJ (2011) Nanomechanics of functional and pathological amyloid materials. Nat Nanotechnol 6:469–479. doi:10.1038/nnano.2011.102

Laura Gambino G, Grassi A, Marletta G (2006) Molecular modeling of interactions between L-lysine and functionalized quartz surfaces. J Phys Chem B 110:4836–4845. doi:10.1021/jp0508610

Lerner EJ (2004) Biomimetic nanotechnology: researchers mimic biology to form nanoscale devices. Ind Phys 10:16–19

Liang FX, Zhang CL, Yang ZZ (2014) Rational Design and Synthesis of Janus Composites. Adv Mater 26:6944–6949. doi:10.1002/adma.201305415

Losev EA, Mikhailenko MA, Achkasov AF, Boldyreva EV (2013) The effect of carboxylic acids on glycine polymorphism, salt and co-crystal formation. A comparison of different crystallisation techniques. New J Chem 37:1973–1981. doi:10.1039/C3NJ41169A

Loskutov AI, Loginov BA, Oshurko VB, Romash EV, Kosheleva NV, Falin AV (2013a) Structural transitions in thin layers of peptide composite materials with silver and gold nanoparticles: influence of temperature and humidity. Nanotechnics (Rus) 2:27–33

Loskutov AI, Uryupina OY, Grigor'ev SN, Oshurko VB, Roldughin VI (2013b) Structure and electrophysical properties of self-organized composite layers based on peptide and silver nanoparticles. Colloid J 75:301–311. doi:10.1134/S1061933X13030113

Loskutov AI, Uryupina OY, Grigor'ev SN, Kosheleva NV, Oshurko VB, Romash EV, Senchikhin IN, Falin AV (2015) Investigation of a structure of new functional peptide composite materials with gold nanoparticles. Prot Met Phys Chem Surf 51:558–566. doi:10.1134/S207020511504022X

Marteel-Parrish AE, Abraham MA (2013) Green chemistry and engineering: a pathway to sustainability. Wiley, Hoboken

Metz B, Kersten GFA, Hoogerhout P, Brugghe HF, Timmermans HAM, de Jong A, Meiring H, ten Hove J, Hennink WE, Crommelin DJA, Jiskoot W (2004) Identification of formaldehyde-induced modifications in proteins reactions with model peptides. J Biol Chem 279:6235–6243. doi:10.1074/jbc.M310752200

Miyazawa T (1960) Normal vibrations of monosubstituted amides in the cis configuration and infrared spectra of diketopiperazine. J Mol Spectrosc 4:155–167. doi:10.1016/0022-2852(60)90075-8

Monti S, Alderighi M, Duce C, Solaro R, Tiné MR (2009) Adsorption of ionic peptides on inorganic supports. J Phys Chem C 113:2433–2442. doi:10.1021/jp809297c

Negishi Y, Tsukuda T (2003) One-pot preparation of sub-nanometer-sized gold clusters via reduction and stabilization by meso-2,3-dimercaptosuccinic acid. J Am Chem Soc 125:4046–4047. doi:10.1021/ja0297483

Philip B (2009) Biosynthesis of Au, Ag and Au–Ag nanoparticles using edible mushroom extract. Spectrochim Acta A 73:374–381. doi:10.1016/j.saa.2009.02.037

Polte J (2015) Fundamental growth principles of colloidal metal nanoparticles—a new perspective. CrystEngComm 17:6809–6830. doi:10.1039/C5CE01014D

Povarnina PY, Vorontsova ON, Gudasheva TA, Ostrovskaya RU, Seredenin SB (2013) Original nerve growth factor mimetic dipeptide GK-2 restores impaired cognitive functions in rat models of Alzheimer's disease. Acta Nat 5:84–91

Prokopovich P, Starov V (2011) Adhesion models: from single to multiple asperity contacts. Adv Colloid Interface Sci 168:210–222. doi:10.1016/i.cis.2011.03.004

Rimola A, Sodupe M, Ugliengo P (2009) Affinity scale for the interaction of amino acids with silica surfaces. J Phys Chem C 113:5741–5750. doi:10.1021/jp811193f

Rimola A, Costa D, Sodupe M, Lambert JF, Ugliengo P (2013) Silica surface features and their role in the adsorption of biomolecules: computational modeling and experiments. Chem Rev 113:4216–4313. doi:10.1021/cr3003054

Rusin M, Ewan BCR, Ristic RI (2013) The glycine-stimulated nucleation and solution-mediated polymorphic transformation of L-glutamic acid. CrystEngComm 15:2192–2196. doi:10.1039/C2CE26344K

Selvakannan PR, Mandal S, Phadtare S, Gole A, Pasricha R, Adyanthaya SD, Sastry M (2004) Water-dispersible tryptophan-protected gold nanoparticles prepared by the spontaneous reduction of aqueous chloroaurate ions by the amino acid. J Colloid Int Sci 269:97–102. doi:10.1016/S0021-9797(03)00616-7

Seredenin SB, Gudasheva TA (2011) Dipeptide mimetics of NGF and BDNF neurotrophins. Patent RUS № 2410392

Sun X, Dong S, Wang E (2006) One-step polyelectrolyte-based route to well-dispersed gold nanoparticles: synthesis and insight. Mat Chem Phys 96:29–33. doi:10.1016/j.matchemphys.2005.06.046

Urupina OY, Vysotskii VV, Loskutov AI, Cherkasova AV, Roldughin VI (2013) Formation of gold nanoparticles in aqueous solutions of cellulose derivatives and a study of the properties of these nanoparticles. Russian J Appl Chem 86:1268–1274. doi:10.1134/S1070427213080193

Venyaminov SYu, Kalnin NN (1990) Quantitative IR spectrophotometry of peptide compounds in water (H_2O) solutions. I. Spectral parameters of amino acid residue absorption bands. Biopolymers 30:1259–1271. doi:10.1002/bip.360301309

Walther A, Müller AHE (2013) Janus particles: synthesis, self-assembly, physical properties, and applications. Chem Rev 113:5194–5261. doi:10.1021/cr300089t

Wang M, Braun HG, Meyer E (2004) Transition of crystal growth as a result of changing polymer states in ultrathin poly(ethylene oxide)/poly(methyl methacrylate) blend films with thickness of <3 nm. Macromolecules 37:437–445. doi:10.1021/ma0355812

Wu S, Yan S, Qi W, Huang R, Cui J, Su R, He Z (2015) Green synthesis of gold nanoparticles using aspartame and their catalytic activity for p-nitrophenol reduction. Nanoscale Res Lett. doi:10.1186/s11671-015-0910-7

Zakaria HM, Shah A, Konieczny M, Hoffmann JA, Nijdam AJ, Reevers ME (2013) Small molecule- and amino acid-induced aggregation of gold nanoparticles. Langmuir 29:7661–7673. doi:10.1021/la400582v